A&A 391, 689–692 (2002)
DOI: 10.1051/0004-6361:20020848

Astronomy & Astrophysics

The early interaction of the planetary nebula NGC 40 with the interstellar medium

J. Martin[1], K. Xilouris[1], and N. Soker[1,2]

[1] University of Virginia, Department of Astronomy, PO Box 3818, Charlottesville, VA 22903-0818, USA
e-mail: jrm7w@virginia.edu; kx8u@virginia.edu
[2] Department of Physics, University of Haifa at Oranim, Tivon 36006, Israel

Received 20 March 2002 / Accepted 6 June 2002

Abstract. We report the detection of an Hα emission-line structure in the upstream side of the planetary nebula NGC 40, which is predicted by numerical simulations, and which is attributed to Rayleigh-Taylor instability. Such a Rayleigh-Taylor instability is expected to occur at early stages of the interaction process between the interstellar medium (ISM) and a fast moving planetary nebula, as is the case for NGC 40. We resolved the Rayleigh-Taylor instability "tongues", as well as the flatness of the nebula around the "tongues", which results from the deceleration by the ISM.

Key words. planetary nebulae: general – ISM: structure – planetary nebulae: individual: NGC 40 – instabilities

1. Introduction

Planetary nebulae (PNe) are expanding ionized nebulae expelled from asymptotic giant branch (AGB) stars. The remnant of the AGB star, i.e., its core, ionizes the nebula as it evolves to become a white dwarf. As the gas expands, its density drops and its expansion starts to be influenced by the ISM. If there is a relative motion between the PN and the ISM, the ISM signature on the PN structure will emerge first on the nebular side facing the ISM, i.e., the upstream direction, where the ISM ram pressure on the nebula is the largest. At late times, when the nebula is relatively large and of low density, this type of interaction forms a bow-shaped nebula, e.g., Sh 2-216 (Tweedy et al. 1995), KeWe 5 (Kerber et al. 1998), KFR 1 (Rauch et al. 2000), and SB 51 (PN G 357.4-07.2; Beaulieu et al. 1999), sometimes with a long extension of the bow-shaped region on the down stream direction, e.g. Abell 35 (Jacoby 1981; Hollis et al. 1996). Since the nebula is large and of low surface brightness at this late stage, telescopes with large fields of view should be used to detect these PNe, as was done by Xilouris et al. (1996) and Tweedy & Kwitter (1996) in their study of many ancient PNe interacting with the ISM. Due to these and other (e.g., Borkowski et al. 1993; Tweedy & Kwitter 1994; Muthu et al. 2000; Kerber et al. 2000, 2002) observational studies, and several theoretical works (e.g., Borkowski et al. 1990; Soker et al. 1991, hereafter SBS; Villaver et al. 2000; Dopita et al. 2000) the basic physics of this stage of PN-ISM interaction is well understood and there are many examples of PNe evolving through this stage.

Send offprint requests to: N. Soker,
e-mail: soker@physics.technion.ac.il

The PN-ISM interaction process may be influenced by the ISM magnetic field (e.g., Soker & Dgani 1997; Soker & Zucker 1997) and several types of instabilities (e.g., SBS; Dgani & Soker 1994; see review by Dgani 2000). Of particular interest is the Rayleigh-Taylor (RT) instability, which may fragment the outer halo, hence allowing the ISM to stream and interact with nebular material closer to the central star (Dgani & Soker 1998). At early stages the RT instability manifests itself as "tongues" located outside, but connected to, the main nebular shell (e.g., SBS; Dopita et al. 2000). This is a general type of structure found in simulations of other dense clouds moving through a low density medium (e.g., Jones et al. 1994). To our best knowledge, no such RT "tongues" were reported before for PNe interacting with the ISM. The only claim for a RT instability at an early stage of PN-ISM interaction was made by Zucker & Soker (1993; hereafter ZS93) for IC 4593. In IC 4593 the nebula is compressed in the upstream direction, such that its density becomes higher, and there is a structure protruding from the nebula in the upstream direction. ZS93 term the region which protrudes from the nebula a "bump". However, in IC 4593 the "bump" is blobby, and does not show any large scale internal structure, i.e., no RT tongues are observed.

In the present paper we report the detection of a structure in the upstream side of the interacting PN NGC 40 (PN G120.0+09.8), which closely resembles the structure of RT instability obtained in numerical simulations. We focus on the RT instability feature, which following ZS93 we term a "bump", although its internal structure reveals features not seen in IC 4593, and which are predicted by numerical simulations. It is quite possible that in NGC 40 the interaction process is at an earlier stage than that of IC 4593. Other properties of

NGC 40 are thoroughly studied by Meaburn et al. (1996), and hence will not be discussed here. In addition to strengthening the theory of PN-ISM interaction, we hope that this first example of a RT instability at very early stages of PN-ISM interaction will stimulate further observations in searching for such features.

2. Observations

Thirty minute exposures were taken of NGC 40 in two narrow band interference filters with the Fan Mountain 40″ Astrometric Telescope on the night of December 4, 2001. The two filters are centered at λ5020 Å, to isolate [OIII] λ5007 Å emission ([OIII] filter), and λ6575 Å, to isolate Hα λ6563 Å and [NII] λ6584 Å emission (Hα filter). The FWHMs (full width at half maximum) of the filters are 53 Å and 68 Å, respectively, and both filters have a throughput of about 70%. The detector is a San Diego State/SITE 2048 × 2048 Engineering grade CCD, and each pixel has a spatial resolution of 0.″36. The images were reduced using the standard procedures of the IRAF data reduction software. Bias subtraction, dome flat field correction, trimsec, and biassec were done. As stated above, we focus only on the outer regions which are dominated by the Hα and [NII] emission, so only the Hα filter image results will be discussed. The effective seeing of the Hα filter image is 1.″8 *FWHM* and the mean airmass during the exposure was 1.21. The IDL routine, "sky", was used to determine the value of the sky in units of ADU/pixel on a region of the chip that is dominated by background and is free of vignetting effects. The image was normalized by subtracting the value of the sky. The subtracted image was then median smoothed by 8 pixels with even interpolation. The median smoothed, subtracted image has a sky value of 0 ± 1ADU/pixel. Our results are presented in Figs. 1a–1e, where the intensity scale is linear.

The RT instability feature is seen on the northwest side of the main (bright) nebular shell. Following ZS93 we term this region the "bump". The ram pressure of the ISM decelerates the expanding gas facing the ISM and flattens the nebula as can be seen in the extended isophotes of Figs. 1b–1e. The limb brightened regions of the bump which are attached to the main nebula, and which are termed "RT-tongues", are indicated in Fig. 1b, as well as the bright clumps that are observed at the front of the bump. Note that the other "blobs" and "filaments" in the images which are scattered around the main nebula have coherence scales much smaller than the size of the "bump" and the flatness to its sides. Such "blobs" are expected to be scattered around PNe, in particular PNe interacting with the ISM (ZS93). The bright blob adjacent to the southwestern edge of the nebula are two close background and/or foreground stars.

Figure 1a shows the light profile along a cut through the bump and between the RT-tongues, as indicated in Fig. 1b. The cut distinctly shows a minimum at $r = 56.''5$, a sharp rise again when it encounters the clumps, and a return to the background as the cut moves into the surrounding ISM. Hints of the RT-tongues are seen in Figs. 2a and 2c of Meaburn et al. (1996). The bent northern jet, a condensation, which may result from the interaction with the ISM, and the direction of proper motion are indicated in Fig. 1d. Note that the condensation ("Cond" in Fig. 1d) does not have the point spread function of the known stars in the field. The proper motion of the central star was measured by the HIPPARCOS mission (Perryman et al. 1997) to be $\mu_\alpha = -8.29 \pm 4.92$ mas yr^{-1}, and $\mu_\delta = 4.36 \pm 4.36$ mas yr^{-1}. The thick arrow indicates the proper motion, while the two thin arrows indicate the extreme 1σ limits of the total proper motion direction.

To demonstrate the similarity of the RT-bump, RT-tongues, and flatness, to the structure obtained in 2D numerical simulations, we show in Fig. 1f the results from SBS, where more details are given (see also Jones et al. 1994 for a very similar RT instability structure). Note that the numerical results present the density in the symmetry plane, while the observations are the integrated emission along line of sight through the nebula. Hence, there is projected emission near the symmetry axis of the interaction flow (tip of the bump) in the Hα images, although no dense material is located there in the simulations.

3. Interaction with the ISM

Prior to our work, there were two indications for the interaction of NGC 40 with the ISM: (i) The bent northern jet (for its detailed structure see Meaburn et al. 1996, and Balick et al. 1992), and (ii) condensations (dense clumps) and filaments around the nebula, i.e., in its halo (Balick et al. 1992), which are thought to be formed from instabilities of the outer low density halo as it interacts with the ISM (ZS93). The proper motion is more or less along the direction expected from the bending angle of the northern jet. These features remind us of IC 4593, which has its northern FLIER (fast low-ionization emission regions along the symmetry axis) closer to the central star than the southern FLIER (ZS93; Corradi et al. 1996), and condensations outside the main nebula (ZS93). We were not surprised therefore to find a "bump" in the direction of proper motion (more or less), as in IC 4593 (ZS93). Whereas in IC 4593 the bump is only suggestive for a RT instability, here the similarity between the bump and the numerical simulations is obvious. For comparison we present in Fig. 1f the density contours map in the symmetry plane from the 2D simulations of SBS. In that figure the nebula is moving upward, with the left edge of the panel being the symmetry axis. The RT instability and the flatness are clearly seen; a similar structure with higher numerical resolution, can be seen in the numerical simulations of a dense cloud moving through a low density medium (Jones et al. 1994, their Fig. 1a). We see in NGC 40 (Figs. 1b–1e) both the RT tongues (which in projection appear as a limb brightened bump) and the flatness of the nebular edge in the upstream direction; this flatness results from the deceleration of the nebular material in the upstream side. We note that the size of the bump is about equal to the deceleration distance of the upstream side, as expected at early stages (SBS). We conclude that the bump is due to RT instability. The detail structure of the bump was influenced by the ionization of the nebula, like is found in numerical simulations for some other nebular features (e.g., Mellema 1995). However, the basic structure seems to result from the RT instability. This can be checked by kinematical study of the bump, which we predict will show variation in velocity on short scales

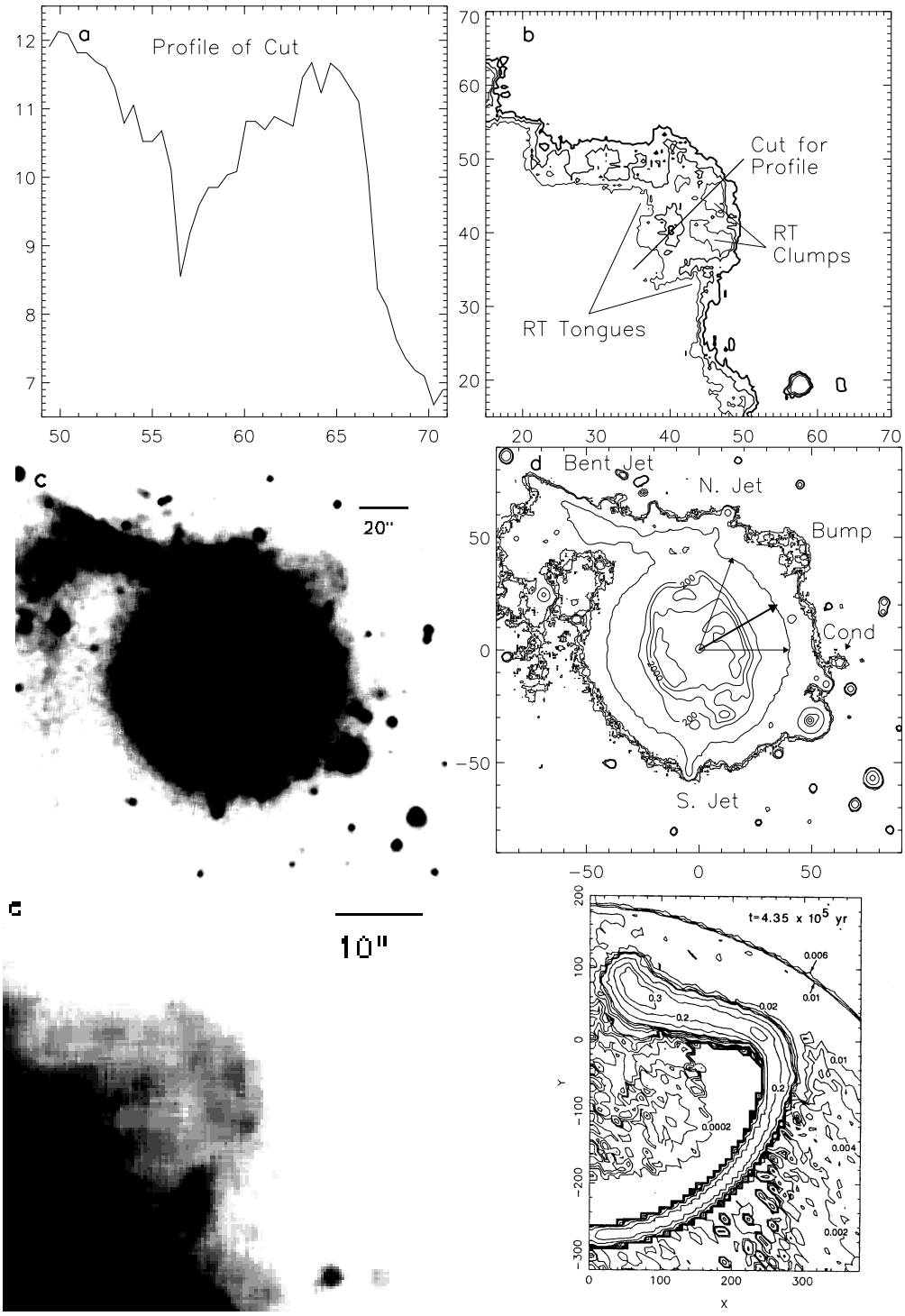

Fig. 1. Mosaic figure emphasizing the Rayleigh-Taylor (RT) instability "bump", and its internal structure with the tongues and clumps. North is up and East is to the left. These features, which are defined on panels **b)** and **d)**, can be clearly seen in panels **c)** and **e)**. **a)** Hα filter intensity vs. distance from the central star in units of arcsec, and along the radial cut marked on panel **b)**. The intensity scale in the images is linear in units of ADU/pixel. **b)** Hα filter surface brightness contour map of the RT "bump" region. The contours have the values (same scale as in panel **a)**) of 9 (dark line), 10 (medium line), and 11 (light line). Axes are distance from the central star in arcsec. **c)** Gray scale image ($180'' \times 180''$). Image is scaled between the values 5 and 50 ADU/pixel. **d)** Hα filter surface brightness contour map of **c)**. The contours have the values of 9, 10, 11, 25, 200, 700, 2000, and 6000. The arrows indicate the direction of the proper motion of the central star. The bold arrow is the direction measured by HIPPARCOS and the lighter arrows indicate the extreme 1σ directions given by the errors in the HIPPARCOS measurement. "Cond" stands for a condensation. Units on the axes are arcsec. **e)** Gray scale of the RT "bump" region of **b)**. Again, the image is scaled between the values 5 and 50 ADU/pixel. **f)** Density contour map for an adiabatic simulation of a dense PN shell from Soker et al. (1991). The nebula is moving upward in this panel, with the left edge of the panel being the symmetry axis of the flow. Contours marked 0.006 and 0.01 indicate the location of the ISM shock front. Units on the axes are 10^{17} cm, and density levels are in units of 10^{-24} g cm^{-1}.

perpendicular to the tongues, with a smoother variation along the tongues.

The condition for the development of the RT instability is that the ISM density be lower than that of the nebula; for that the ISM should be hotter than the nebula (SBS; we follow their analysis). SBS assume that the nebula is at a temperature of $\sim 10^4$ K, and calculate the cooling time of the hot shocked ISM to that temperature (SBS). The cooling time depends on the relative velocity of the ISM and the nebula, and on the density and ionization stage of the ISM. For the angular proper motion given in the previous section and a distance of 980 ± 100 pc to NGC 40 (Bianchi & Grewing 1987), the transverse motion is $v_{\rm t} \sim 44 \pm 30$ km s^{-1}. The heliocentric radial velocity of NGC 40 is $v_{\rm r} = -32$ km s^{-1} (Meaburn et al. 1996). The absolute value of the velocity of NGC 40 relative to the sun is therefore $v_* = (v_{\rm r}^2 + v_{\rm t}^2)^{1/2} \simeq 54$ km s^{-1}. For a nebular expansion velocity of $v_{\rm e} = 10$ km s^{-1}, and neglecting the ISM motion, we find for the relative velocity between the nebular gas and the ISM, $v_{\rm rel} = v_* + v_{\rm e} \sim 64$ km s^{-1}. We can safely take then $v_{\rm rel} = 60$ km s^{-1}. We assume that NGC 40 is moving in the warm ionized medium, for which the average hydrogen number density at the location of NGC 40, namely 170 pc from the galactic plane, is <0.05 cm^{-3} (Reynolds 1989). The ISM is shocked to a temperature of $\sim 5 \times 10^4$ K, from which the cooling time to a temperature of $\sim 10^4$ K is $t_{\rm cool} \sim 3{\times}10^4 (n_{\rm o}/0.05\,{\rm cm}^{-3})^{-1}$ yr. The radius of the NGC 40 (at the location of the bump) is 1′, or $R_{\rm PN} = 9 \times 10^{17}$ cm, assuming a distance of 1 kpc to NGC 40. The flow time of the ISM along a distance of $R_{\rm PN}$, and for $v_* = 50$ km s^{-1}, is $t_{\rm flow} \sim 6 \times 10^3$ yr. Since $t_{\rm cool} > t_{\rm flow}$, the ISM has no time to cool and an adiabatic flow, prone to RT instability, commences (SBS). In addition, at a very early stage, before the nebula is ionized, its temperature is $\lesssim 10^3$ K, so even if the ISM cools faster down to $\sim 10^4$ K, its cooling will be slower below that temperature, and the ISM will be hotter and less dense than the nebular gas at early stages. The expansion time of the material in the bump, since it left the central star, is $R_{\rm pn}/v_{\rm e} \simeq 3 \times 10^4$ yr, long enough for the development of a RT instability bump (SBS).

To conclude, NGC 40 is moving through, and interacting with, the ISM. The motion and indication for this interaction were known previously. We report for the first time the detection of a structure on the upstream edge of the main nebula which is predicted by numerical simulations, and which is attributed to RT instability at an early stage of the interaction process. Such a RT instability is expected to occur at early stages of the PN-ISM interaction under conditions similar to those for NGC 40.

Acknowledgements. We thank Robert O'Connell for valuable comments on the original manuscript. J. M. was supported by the NASA Long Term Space Astrophysics grant NAG5-6403. N. S. was supported by a Celerity Foundation Distinguished Visiting Scholar grant at the University of Virginia, and by a grant from the US-Israel Binational Science Foundation.

References

Balick, B., Gonzalez, G., Frank, A., & Jacoby, G. 1992, ApJ, 392, 582
Beaulieu, S. F., Dopita, M. A., & Freeman, K. C. 1999, ApJ, 515, 610
Bianchi, L., & Grewing, M. 1987, A&A, 181, 85
Borkowski, K. J., Sarazin, C. L., & Soker, N. 1990, ApJ, 360, 173
Borkowski, K. J., Tsvetanov, Z., & Harrington, J. P. 1993, ApJ, 402, L57
Corradi, R. L. M., Manso, R., Mampaso, A., & Schwarz, H. E. 1996, A&A, 313, 913
Dgani, R. 2000, in Asymmetrical Planetary Nebulae II: From Origins to Microstructures, ed. J. H. Kastner, N. Soker, & S. Rappaport (San Francisco: ASP), ASP Conf. Ser., 199, 305
Dgani, R., & Soker, N. 1994, ApJ, 434, 262
Dgani, R., & Soker, N. 1998, ApJ, 495, 337
Dopita, M. A., Massaglia, S., Bodo, G., Arnaboldi, M., & Merluzzi, P. 2000, in Asymmetrical Planetary Nebulae II: From Origins to Microstructures, ed. J. H. Kastner, N. Soker, & S. Rappaport (San Francisco: ASP), ASP Conf. Ser., 199, 423
Hollis, J. M., van Buren, D., Vogel, S. N., et al. 1996, ApJ, 456, 644
Jacoby, G. H. 1981, ApJ, 244, 903
Jones, T. W., Kang, H., & Tregillis, I. L. 1994, ApJ, 432, 194
Kerber, F., Furlan, E., Rauch, T., & Roth, M. 2000, in Asymmetrical Planetary Nebulae II: From Origins to Microstructures, ed. J. H. Kastner, N. Soker, & S. Rappaport (San Francisco: ASP), ASP Conf. Ser., 199, 313
Kerber, F., Guglielmetti, F., Mignani, R., & Roth, M. 2002, A&A, 381, L9
Kerber, F., Roth, M., Manchado, A., & Groebner, H. 1998, A&AS, 130, 501
Meaburn, J., Lopez, J. A., Bryce, M., & Mellema, G. 1996, A&A, 307, 579
Mellema, G. 1995, MNRAS, 277, 173
Muthu, C., Anandarao, B. G., & Pottasch, S. R. 2000, A&A, 355, 1098
Perryman, M. A. C., Lindegren, L., Kovalevsky, J., et al. 1997, A&A, 323, L49
Rauch, T., Furlan, E., Kerber, F., & Roth, M. 2000, in Asymmetrical Planetary Nebulae II: From Origins to Microstructures, ed. J. H. Kastner, N. Soker, & S. Rappaport (San Francisco: ASP), ASP Conf. Ser., 199, 341
Reynolds, R. J. 1989, ApJ, 339, L29
Soker, N., Borkowski, K. J., & Sarazin, C. L. 1991, AJ, 102, 1381 (SBS)
Soker, N., & Dgani, R. 1997, ApJ, 484, 277
Soker, N., & Zucker, D. B. 1997, MNRAS, 289, 665
Tweedy, R. W., & Kwitter, K. B. 1994, AJ, 108, 188
Tweedy, R. W., & Kwitter, K. B. 1996, ApJS, 107, 255
Tweedy, R. W., Martos, M. A., & Noriega-Crespo, A. 1995, ApJ, 447, 257
Villaver, E., Manchado, A., & García-Segura, G. 2000, RMxAC, 9, 213
Xilouris, K. M., Papamastorakis, J., Paleologou, E., & Terzian, Y. 1996, A&A, 310, 603
Zucker, D. B., & Soker, N. 1993, ApJ, 408, 579 (ZS93)